POLITECNICO DI TORINO
Repository ISTITUZIONALE

Numerical Tool Optimization for Advanced Rocket Nozzle Performance Prediction

*Original*
Numerical Tool Optimization for Advanced Rocket Nozzle Performance Prediction / Conte, Antonietta; Ferrero, Andrea; Larocca, Francesco; Pastrone, Dario Giuseppe. - ELETTRONICO. - (2019). (Intervento presentato al convegno AIAA Propulsion and Energy 2019 Forum tenutosi a Indianapolis (USA) nel 19-22 August 2019) [10.2514/6.2019-4115].

*Availability:*
This version is available at: 11583/2750894 since: 2020-05-12T11:27:57Z

*Publisher:*
AIAA

*Published*
DOI:10.2514/6.2019-4115

*Terms of use:*

This article is made available under terms and conditions as specified in the corresponding bibliographic description in the repository

*Publisher copyright*

(Article begins on next page)

23 April 2024

AIAA Propulsion and Energy Forum
19-22 August 2019, Indianapolis, IN
AIAA Propulsion and Energy 2019 Forum

10.2514/6.2019-4115

Check for updates

# Numerical Tool Optimization for Advanced Rocket Nozzle Performance Prediction

Antonietta Conte*, Andrea Ferrero†, Francesco Larocca ‡, Dario Pastrone§
*Politecnico di Torino, Torino, Italy, 10129*

**A number of Altitude-Compensating Nozzle concepts have been developed through the years, to reduce nozzle performance losses. One of the most promising concepts is the dual-bell nozzle, where the flow is capable of auto-adapting at low and high altitude without the use of mechanical devices. This paper focuses on the optimization and validation of an in-house solver for the prediction of the flow field in advanced rocket nozzles, with emphasis on dual-bell rocket nozzles. Numerical efforts are concentrated on predicting transition from one operating mode to the other, since low and high altitude operating modes are both well known stable conditions. Both steady state and transient problems are considered and the performances of different numerical schemes are investigated.**

## Nomenclature

| | | |
|---|---|---|
| $CFL$ | = | Courant-Friedrichs-Lewy number, |
| $p_a$ | = | Ambient static pressure, |
| $p_w$ | = | Wall static pressure, |
| $p_c$ | = | Chamber total pressure, |
| $NPR$ | = | $= p_c/p_a$, Nozzle Pressure Ratio, |
| $R_t$ | = | Throat radius, |
| $x_{sep}$ | = | Separation point location (with respect to throat) |

## I. Introduction

Conventional bell nozzles feature a single adaptation altitude and maximum performance cannot be achieved along the whole trajectory. Launcher first-stage engines operate in an environment with varying pressure, from sea-level to nearly vacuum conditions. Different nozzle concepts have been studied with the aim of closing the gap between conventional and ideal engines, improving the average thrust coefficient, launcher performance and the relative payload mass [1, 2]. The dual-bell nozzle stands out amongst the most promising ideas. Dual-bell nozzles were first introduced in the United States in 1949 [3, 4]. The concept is based on an altitude-compensating nozzle that merges two conventional bell-shaped nozzles with different contour geometries and expansion ratios. The geometrical discontinuity of the nozzle profile allows two different operating modes or adapted conditions, depending on the ambient conditions. Controlled separation is achieved at low altitude, since the flow is attached to the first contour and separates at the inflection point. The separation point remains at the inflection point for a wide range of nozzle pressure ratios, due to the strong pressure gradient at the inflection point. When flow separation occurs, lower side loads than in overexpanded conventional bell nozzles are generated, since chamber and ambient perturbations induce only weak displacements of the separation point. At high altitudes, the flow is attached to the whole divergent contour. The limitation of nozzle expansion ratio caused by sea level operation can therefore be circumvented, and, consequently, a higher vacuum specific impulse will be obtained with respect to classical bell nozzles that feature a single adaptation altitude.

Many numerical and experimental studies have been performed over the years to investigate the advantages and disadvantages of dual-bell nozzles. Despite the aforementioned advantages, there may be performance losses due to early transitions from the first to the second operative mode [5]. Several studies have been performed to analyze

*PhD Student, Department of Mechanical and Aerospace Engineering, Corso Duca degli Abruzzi 24, Torino, Italy
†Assistant Professor, Department of Mechanical and Aerospace Engineering, Corso Duca degli Abruzzi 24, Torino, Italy, AIAA Member
‡Associate Professor, Department of Mechanical and Aerospace Engineering, Corso Duca degli Abruzzi 24, Torino, Italy
§Full Professor, Department of Mechanical and Aerospace Engineering, Corso Duca degli Abruzzi 24, Torino, Italy, AIAA Associated Fellow.

Downloaded by Antonietta Conte on September 10, 2019 | http://arc.aiaa.org | DOI: 10.2514/6.2019-4115

Copyright © 2019 by Antonietta Conte, Andrea Ferrero, Francesco Larocca, Dario Pastrone.
Published by the American Institute of Aeronautics and Astronautics, Inc., with permission.

in depth their flow field characteristics, separation transition and hysteresis, with the aim of establishing a transition prediction model. Experimental and numerical research has been conducted to optimize the transitional behavior through the variation of the extension geometry, such as [6, 7]. In particular, the unsteady behavior observed during the transition is characterised by the presence of hysteresis phenomena [8].
Several studies [5–7, 9] found that a contour extension featuring a positive pressure gradient leads to a wide range of hysteresis and so a better stability of the operational modes. Sneak transition length and duration are also influenced by the wall pressure gradient. The preliminary results available in the literature support the adoption of this technology, even if further investigation is necessary to better understand the transition features between the two operating modes, improve the geometry design and make this technology a practical alternative to conventional nozzles.

In the present work an in-house CFD code is tested on different nozzle configurations with the aim of validating and optimizing the code, which can then be used for future studies on advanced nozzle concepts. The code offers the possibility to integrate the governing equations by means of several spatial and temporal discretization methods in both 2D and 3D domains: the different approaches are investigated and a comparison with the available experimental data is reported.

Downloaded by Antonietta Conte on September 10, 2019 | http://arc.aiaa.org | DOI: 10.2514/6.2019-4115

## II. Numerical framework

The numerical simulations reported in this work are performed by an in-house computational fluid dynamics solver. Several physical models (Euler, Navier-Stokes, Reynolds Averaged Navier-Stokes (RANS)) have been implemented and tested and the numerical results have been compared with the experimental data for different applications (with both internal and external flows [10–16]) in order to understand the range of applicability of the code. The focus of this work is on the optimization and validation of the solver for simulating cold-flow nozzles as a first step to the study of advanced nozzle concepts. All the results presented in the following are obtained by the integration of the 2D axisymmetric RANS equations with the Spalart-Allmaras [17] turbulence closure. The code can manage both Discontinuous Galerkin finite element and finite volume spatial discretization in a parallel environment based on the Message Passing Interface (MPI) approach. The time integration can be performed with both explicit and implicit schemes.

### A. Discontinuous Galerkin finite element spatial discretization

The Discontinuous Galerkin (DG) finite element discretization allows to easily manage unstructured meshes in a parallel environment. The basic idea behind DG methods is to introduce several degrees of freedom inside each element in order to perform arbitrary high-order reconstructions simply by using the data available inside the element. This simplifies the implementation in the presence of non-conforming meshes with hanging nodes (for example at the interface between the stator mesh and rotor mesh in turbomachinery problems). Furthermore, the fact that the reconstruction does not require data from the neighbouring elements makes the scheme quite robust in the presence of distorted and irregular meshes.
The solution inside each element is here described by means of an orthonormal and hierarchical modal basis obtained by the application of the modified Gram-Schmidt procedure to a set of monomials defined in the physical space, following the approach of [18]. Several numerical fluxes have been implemented for the computation of convective fluxes, like for example the local Lax-Friedrichs or Rusanov flux [19], the AUSM+ [20] and the Flux Difference Splitting based on an approximate Riemann problem solver [21]. Diffusive fluxes are computed by means of a recovery-based approach [15].
The simulation of compressible flows characterized by the presence of shock waves requires the introduction of a shock-capturing strategy. Several approaches have been implemented in the code: limiters based on the Barth-Jespersen approach in a DG framework [22], adaptive filtering [11] and diffent artificial viscosity methods [23–25].
The management of the unstructured mesh in the MPI parallel environment is performed through the DMPlex class [26] provided by the PETSc library [27].

### B. Finite volume spatial discretisation

The DG method can be seen as a high-order extension of a finite volume (FV) method. If the reconstruction order inside a DG element is reduced so that a single mode (the average value) is kept in the basis then a first order FV method is obtained. For this reason, the code offers the possibility to work also in a FV framework. When this approach is chosen, the reconstruction required to compute the diffusive fluxes is performed by means of a weighted least squares

approach. As far as the reconstruction required by the convective terms is concerned it is possible to adopt a constant reconstruction (first order scheme) or a linear reconstruction (second order scheme) inside each element. When the linear reconstruction is chosen, an unstructured limiter is employed.

### C. Time integration

Both explicit and implicit time integration schemes have been implemented. Different accuracy orders are available for the explicit time integration schemes: first order Euler scheme, second and third order RK TVD schemes [28] and fourth order Strong-Stability Preserving Runge-Kutta 4 [29] scheme. As far as the implicit time integration is concerned, only a linearised first order backward Euler scheme has been implemented. The resulting linear system is solved in parallel by the GMRES algorithm with the Additive Schwarz preconditioner provided by the PETSc library [27]. The Jacobian matrix required by the implicit scheme can be computed both numerically or analytically (for example by means of the Tapenade automatic differentiation tool [30]). In this work, a numerically evaluated Jacobian is used because the code is currently under development and the numerical approach automatically takes into account any modifications in the source code.

Downloaded by Antonietta Conte on September 10, 2019 | http://arc.aiaa.org | DOI: 10.2514/6.2019-4115

## III. Numerical results on bell shaped nozzles

First of all, some numerical tests were performed on classical bell nozzles for values of Nozzle Pressure Ratio (NPR) which are characterized by flow separation. In particular, both parabolic (PAR) and truncated ideal contour (TIC) nozzles were considered. Experimental data and geometries for cold flow tests are available for these configurations, from the work of J. H. Ruf et al. [31] and Stark and Hagemann [32], respectively. The simulations were carried out by using the solver in DG mode with a second order accurate spatial discretization (DG1) and explicit time integration. The Spalart-Allmaras turbulence model [17] was adopted. Shock capturing was performed by means of modal filtering [11]. The results reported in Figure 1 show the Mach field and the wall pressure distribution for the studied PAR (NPR=16, 21.44) and TIC (NPR=25.25) nozzle, respectively. The TIC test case was the subject of an international comparison in which several RANS models (Spalart-Allmaras,$k-\omega$, SST) were investigated [32]: the results of the comparison showed that RANS predictions are characterized by a large uncertainty on the prediction of the separation point location $x_{sep}$. The range of variation of the separation point predicted during this comparison is reported in Figure 1b by black solid lines: the results of the present study falls inside this range.

## IV. Numerical results on dual-bell nozzle

The flow in the dual-bell nozzle experimentally and numerically studied by Schneider and Génin [33] was numerically investigated by the solver under development. The nozzle consists in a first bell designed as a Truncated Ideal Contour (TIC) followed by a second bell with a parabolic increasing pressure profile. The geometry used for the simulations was obtained by joining the first bell contour with an approximation of the second bell obtained by a parabolic fitting of the geometry published in [33]. Furthermore, the end of the nozzle was smoothed by introducing a small curvature radius, as shown in Figure 2b. In Figure 2a it is also possible to see the full computational domain. Far field boundary conditions were set at $200R_t$ and $50R_t$ in the axial and radial directions, respectively. The mesh was generated by Gmsh [34] with the Frontal-Delaunay for quads algorithm. It contains 170000 elements.
The simulations were carried out by using the solver in finite volume mode. Time integration was performed by means of the implicit Euler scheme. For steady simulations, the CFL number was chosen automatically at each time step by following the pseudo-transient continuation strategy [35] and setting $10^1 \leq CFL \leq 10^3$.

In Figure 3 it is possible to compare the Mach number obtained for the steady simulations at $NPR = 20, 30, 48$ and 60, respectively. The predicted wall pressure distribution is compared to the available experimental data in Figure 4. The plot shows that the numerical results at NPR=48 are quite close to the experimental values while a larger discrepancy is observed at NPR=30. This discrepancy is larger with respect to the numerical results reported in [33]: this could be due to the fact that an approximated geometry was used in the present work. Furthermore, a local refinement of the mesh in the region of the inflection points could improve the results.
In order to evaluate the unsteady behavior of the dual-bell nozzle and to highlight the hysteresis related to the transition between the low-altitude and high-altitude working modes, unsteady simulations were performed. In the first simulation, the NPR was increased from 20 to 60 with a constant inlet total pressure gradient ($dp_c/dt = 2.5$ bar/ms). This gradient is in line with the value chosen by Schneider and Génin [33] for a numerical unsteady analysis of this dual-bell nozzle.

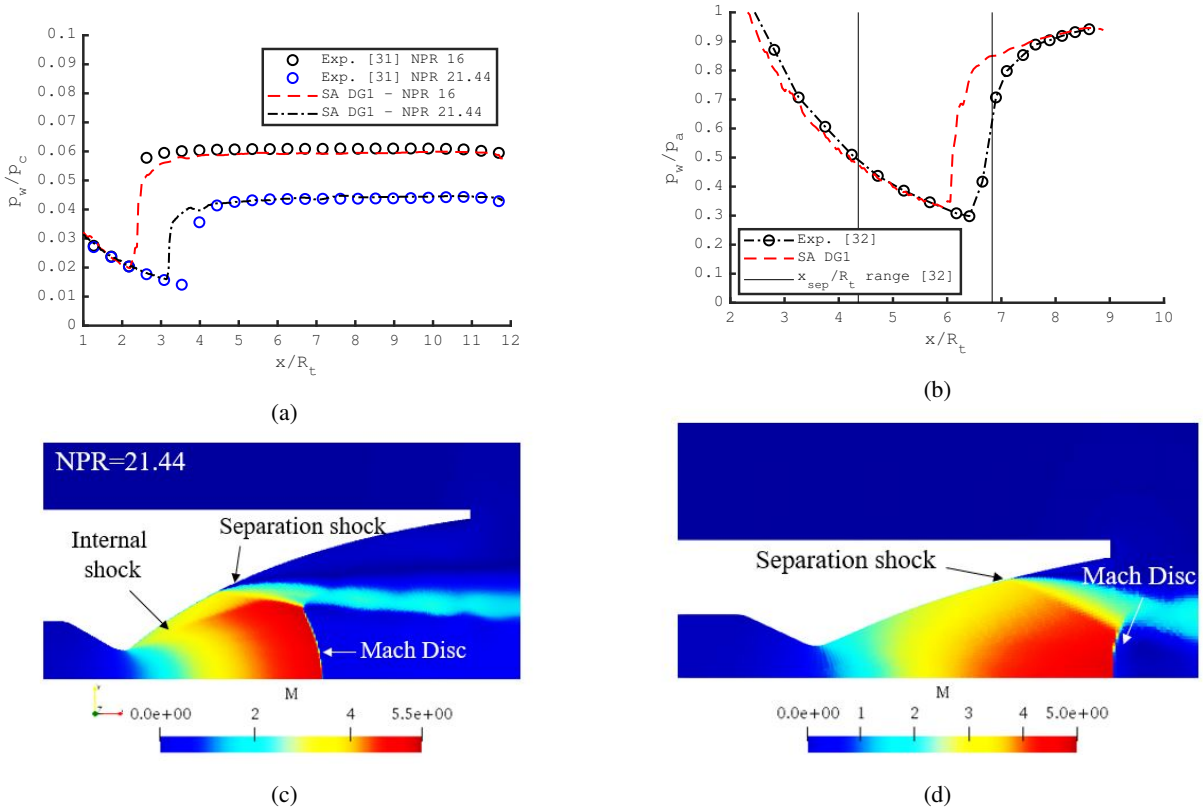


**Fig. 1 Wall pressure distribution and Mach number field for PAR (a,c) and TIC (b,d) nozzles.**

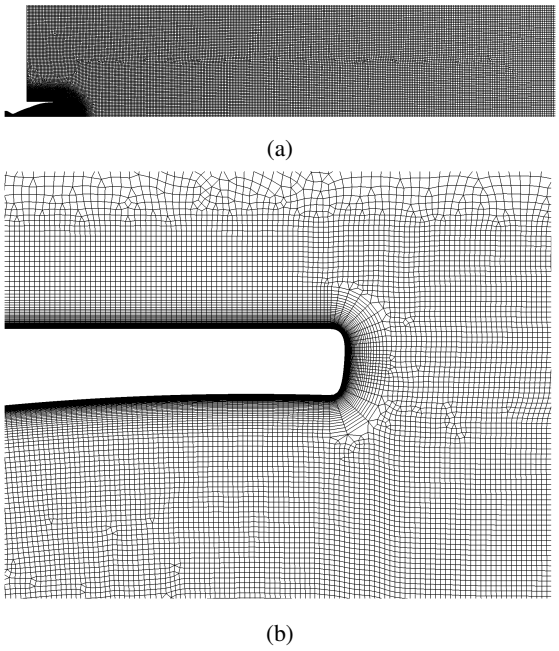


**Fig. 2 Computational mesh (a) and detail of the exit section (b)**

Downloaded by Antonietta Conte on September 10, 2019 | http://arc.aiaa.org | DOI: 10.2514/6.2019-4115

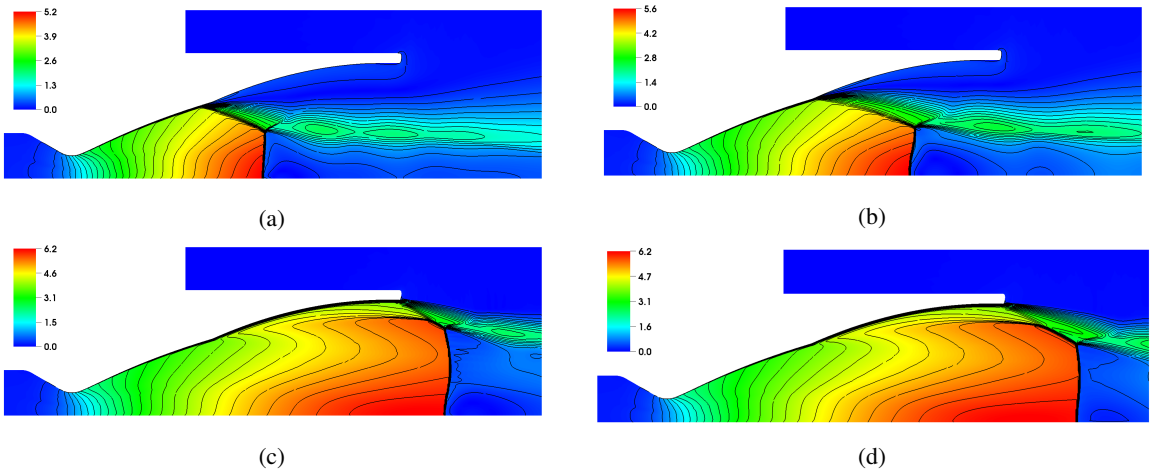


**Fig. 3 Mach field for dual-bell nozzle at NPR=20 (a), NPR=30 (b), NPR=48 (c) and NPR=60 (d).**

In particular, they performed a convergence study on the time step size and observed that almost no influence can be noticed when the time step size is varied in the range $5 \times 10^{-7} s \leq dt \leq 10^{-5} s$. For this work, a time step size equal to $6 \cdot 10^{-7} s$ was adopted. This value corresponds to a CFL number approximately equal to 200.
A second unsteady simulation was performed by decreasing the $NPR$ from 60 to 20, with the same pressure gradient magnitude.
The same analysis was also repeated with a smaller pressure gradient ($dp_c/dt$ = 1.25 bar/ms). The results of these simulations are reported in Figure 5 where the position of the separation point is reported as a function of the instantaneous NPR: the hysteresis phenomenon is clearly noticeable. The plot also shows that the extension of the hysteresis region grows with the magnitude of the pressure gradient.

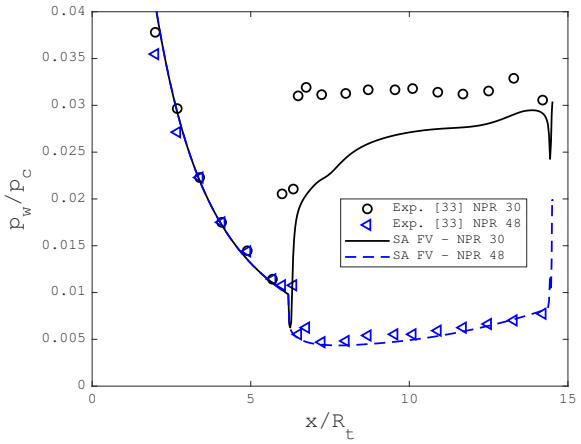


**Fig. 4 Wall pressure distribution in dual-bell nozzle.**

## V. Comparison of different numerical schemes

The first simulations performed for this work and reported in Section III were performed by using a DG spatial discretization. When the code works in this mode, a shock capturing approach should be chosen between limiters, filtering and artificial viscosity. Some preliminary tests showed that both limiters and filters can effectively stabilize the simulation without destroying the accuracy of the reconstruction. However, when limiters and filters are applied in a DG framework they are usually implemented as a post-processing step which should be applied at the end of each time



Downloaded by Antonietta Conte on September 10, 2019 | http://arc.aiaa.org | DOI: 10.2514/6.2019-4115

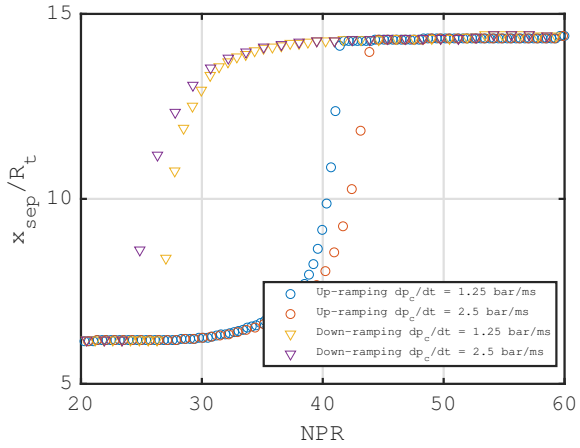


**Fig. 5 Hysteresis in transient simulations for dual-bell nozzle.**

step. For this reason, limiters and filters can easily be adopted together with explicit time integration schemes. However, they are not sufficient to stabilize the numerical solution when implicit time integration with large time steps is adopted, because they do not introduce any stabilizing effect in the Jacobian matrix. In contrast, artificial viscosity can easily be applied together with implicit time integration schemes, because it introduces some stabilizing terms in the discretized equations and these terms appear in the Jacobian matrix of the implicit scheme. However, the authors observed that it is difficult to find an artificial viscosity term able to stabilize the solution without introducing unphysical effects when the solution is not completely resolved. The problems under investigation are characterized by strong shock waves with separated flows at very high Reynolds number (typically $10^7 - 10^8$ considering the throat radius, the stagnation speed of sound, the stagnation density and the stagnation viscosity). In particular, some portions of the boundary layers in the convergent and close to the throat are usually under-resolved: some tests show that in these regions the artificial viscosity becomes active and, in this case, can significantly alter the magnitude of the turbulent eddy viscosity.
For these reasons, the DG solutions reported in this work were obtained by explicit time integration. However, explicit time integration is particularly expensive in problems where a high Reynolds number leads to the use of very small cells at wall. In order to perform implicit time integration, the solver is used in finite volume mode with shock capturing based on slope limiters. This is due to the fact that the limiters in a finite volume scheme take part to the reconstruction process and so their stabilizing effect is included in the Jacobian matrix of the implicit time integration scheme.

In order to correctly compare the performances of explicit and implicit time integration schemes it is necessary to take into account not only the time step size but also the cost of the single step. For this reason, a test was performed in order to measure the computational time required by the different schemes to simulate the transient dual-bell problem. The tests were carried out with 20 MPI processes on a workstation equipped with an Intel Xeon E5-2600 v4 processor. The results are reported in Tab. 1 in which the explicit Euler scheme (with $CFL = 0.6$) is compared with the implicit Euler scheme ($CFL = 10^1, 10^2, 10^3$). The Table shows the ratio between the required computational time in seconds ($\Delta t_{CPU}$) and the physical computational time in seconds ($\Delta t_{phys}$). These results are valid only for this problem with the chosen mesh resolution since the time step size is determined by the size of the cells which can be very small close to the wall at the considered Reynolds number.
The relative speed of the implicit scheme with respect to the explicit scheme grows quickly with the CFL number. For example, the dual bell transient simulation from $NPR = 20$ to $NPR = 60$ with $dp_c/dt = 2.5$bar/ms requires to simulate a physical interval equal to 0.016s: if this simulation is performed on the workstation used for the tests, the computation requires 4 hours with the implicit scheme (with $CFL = 10^3$) and 47 days with the explicit scheme.
It is possible to notice that the cost of the implicit scheme is not exactly inversely proportional to the $CFL$ number: this is due to the fact that when larger $CFL$ values are chosen, the GMRES algorithm needs to perform more iterations during each time step in order to solve the linear system up to the required tolerance. Furthermore, it is useful to remember that the Jacobian matrix required by the implicit solver is here evaluated numerically because the code is under development and the numerical approach allows to automatically keep into account any update in the source code. A simple profiling analysis showed that, in the present problem, 70 % of the computational time required by one step of

Downloaded by Antonietta Conte on September 10, 2019 | http://arc.aiaa.org | DOI: 10.2514/6.2019-4115

the implicit solver is required to compute numerically the Jacobian matrix (with $CFL = 10^3$). For this reason, great improvements can be obtained by switching to an analytical evaluation of the Jacobian matrix.

| | Expl. $CFL = 0.6$ | Impl. $CFL = 10^1$ | Impl. $CFL = 10^2$ | Impl. $CFL = 10^3$ |
|---|---|---|---|---|
| $\Delta t_{CPU}/\Delta t_{phys}$ | 2.54E+08 | 7.37E+07 | 7.45E+06 | 9.03E+05 |
| Relative speed w.r.t. explicit | 1.00 | 3.45 | 34.1 | 281 |

**Table 1 Computational cost of explicit and implicit schemes for transient dual-bell problem**

Finally, the parallel performances of the solver have been tested and optimized. The purpose of this analysis is to understand the feasibility of future unsteady studies based on LES or hybrid RANS-LES approaches. In particular, the results of two weak scalability tests are reported in Figure 6. The first test refers to a 3D Large Eddy Simulation performed with a third order accurate DG scheme and second order accurate explicit time integration. This test was performed on the cluster Marconi at CINECA, which is equipped with Intel KNL processors (68 cores per processor). The number of degrees of freedom per core is $2 \cdot 10^5$. The results in Figure 6 show that good scalability performances were obtained up to 4000 cores.
A second test was performed on a 2D RANS problem with implicit time integration. The test was performed on an x86 cluster equipped with Intel Xeon E5-2680 processors (12 cores per processor). The number of degrees of freedom per core is in line with the values used for the nozzle simulations considered in this work ($4 \cdot 10^4$). The plot in Figure 7 shows that the present implementation of the implicit time integration scheme has lower scalability potential with respect to the explicit time integration scheme. Future work will be devoted to improve both the serial and parallel performances of this preliminary implementation.

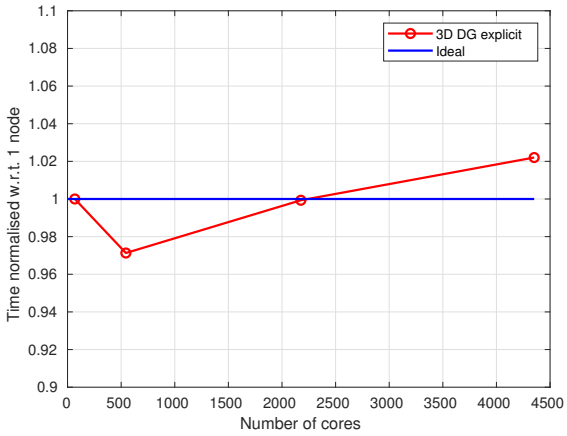


**Fig. 6 Weak scalability test for 3D third order accurate DG simulation with explicit time integration on Marconi KNL (68 cores per node)**

## VI. Conclusions

A research CFD code was tested on the prediction of separated flows in both conventional and dual-bell rocket nozzles. The solver was tested in both DG and FV modes. The computational cost of both explicit and implicit time integration schemes has been presented, showing the great benefits related to the use of implicit time integration in the considered class of problems. The parallel performances of the solver were also investigated, showing that massive parallelization can be easily obtained with explicit time integration while the implicit scheme shows good scalability for smaller numbers of cores. However, the nozzle flows investigated in this work are described by 2D axisimmetryc RANS equations: the small size of the problem makes implicit time integration the best solution for these problems



Downloaded by Antonietta Conte on September 10, 2019 | http://arc.aiaa.org | DOI: 10.2514/6.2019-4115

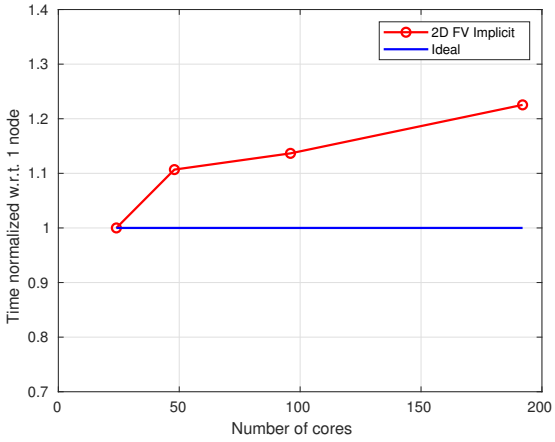


**Fig. 7 Weak scalability test for 2D second order accurate FV simulation with implicit time integration on x86 cluster (24 cores per node)**

since it is not necessary to adopt massive parallelization.

## Acknowledgments

Computational resources were provided by HPC@POLITO (http://www.hpc.polito.it). We acknowledge the CINECA award under the ISCRA initiative, for the availability of high performance computing resources and support: the scalability results on the Marconi cluster were obtained during the class C project TENORE.
The authors would like to thank F. Nasuti and E. Martelli for their suggestions, constructive remarks and for providing the TIC geometry for the dual-bell nozzle.

## References

[1] Boccaletto, L., and J.-P.Dussauge, "High-Performance Rocket Nozzle Concept," *Journal of Propulsion and Power*, Vol. 26, No. 5, 2010, pp. 969–979.

[2] Casalino, L., Pastrone, D., and Simeoni, F., "Effects of Limitation of Nozzle Flow Separation on Launcher Performance," *Journal of Propulsion and Power*, Vol. 29, No. 4, 2013, pp. 849–854.

[3] Hagemann, G., Immich, H., Nguyen, T. V., and Dumnov, G. E., "Advanced rocket nozzles," *Journal of Propulsion and Power*, Vol. 14, No. 5, 1998, pp. 620–634. doi:10.2514/2.5354.

[4] Foster, C. R., and Cowles, F. B., "Experimental Study of Gas-Flow Separation in Overexpanded Exhaust Nozzles for Rocket Motors," Progress rept. 4-103, Jet Propulsion Laboratory, California Inst. of Technology, Pasadena, CA, May 1949.

[5] Frey, M., and Hagemann, G., "Critical assessment of dual-bell nozzles," *Journal of propulsion and power*, Vol. 15, No. 1, 1999, pp. 137–143.

[6] Nasuti, F., Onofri, M., and Martelli, E., "Role of wall shape on the transition in axisymmetric dual-bell nozzles," *Journal of propulsion and power*, Vol. 21, No. 2, 2005, pp. 243–250. doi:10.2514/1.6524.

[7] Génin, C., Stark, R., Haidn, O., Quering, K., and Frey, M., "Experimental and Numerical Study of Dual Bell Nozzle Flow," *Progress in Flight Physics*, Vol. 5, 2013, pp. 363–376.

[8] Nasuti, F., Onofri, M., and Martelli, E., "Numerical Study of Transition between the two operating modes of Dual-bell nozzles," *38th AIAA/ASME/SAE/ASEE Joint Propulsion Conference & Exhibit*, 2002, p. 3989.

[9] Martelli, E., Nasuti, F., and Onofri, M., "Numerical analysis of film cooling in advanced rocket nozzles," *AIAA journal*, Vol. 47, No. 11, 2009, pp. 2558–2566.

Downloaded by Antonietta Conte on September 10, 2019 | http://arc.aiaa.org | DOI: 10.2514/6.2019-4115

[10] Ferrero, A., Iollo, A., and Larocca, F., "Global and local POD models for the prediction of compressible flows with DG methods," *International Journal for Numerical Methods in Engineering*, Vol. 116, No. 5, 2018, pp. 332–357. doi:10.1002/nme.5927.

[11] Ferrero, A., and Larocca, F., "Feedback filtering in discontinuous Galerkin methods for Euler equations," *Progress in Computational Fluid Dynamics, an International Journal*, Vol. 16, No. 1, 2016, pp. 14–25. doi:10.1504/PCFD.2016.074221.

[12] Ampellio, E., Bertini, F., Ferrero, A., Larocca, F., and Vassio, L., "Turbomachinery design by a swarm-based optimization method coupled with a CFD solver," *Advances in aircraft and spacecraft science*, Vol. 3, No. 2, 2016, pp. 149–170. doi: 10.12989/aas.2016.3.2.149.

[13] Ferrero, A., and Larocca, F., "Adaptive CFD schemes for aerospace propulsion," *Journal of Physics: Conference Series*, Vol. 841, No. 1, 2017. doi:10.1088/1742-6596/841/1/012017.

[14] Ferrero, A., Larocca, F., and Bernaschek, V., "Unstructured discretisation of a non-local transition model for turbomachinery flows," *Advances in aircraft and spacecraft science*, Vol. 4, No. 5, 2017, pp. 555–571. doi:10.12989/aas.2017.4.5.555.

[15] Ferrero, A., Larocca, F., and Puppo, G., "A robust and adaptive recovery-based discontinuous Galerkin method for the numerical solution of convection–diffusion equations," *International Journal for Numerical Methods in Fluids*, Vol. 77, No. 2, 2015, pp. 63–91. doi:10.1002/fld.3972.

[16] Ferrero, A., and Pastrone, D., "Plasma Actuator–Assisted Rocket Nozzle for Improved Launcher Performance," *AIAA Journal*, Vol. 57, No. 4, 2019, pp. 1348–1354.

[17] Allmaras, S. R., and Johnson, F. T., "Modifications and clarifications for the implementation of the Spalart-Allmaras turbulence model," *Seventh international conference on computational fluid dynamics (ICCFD7)*, 2012, pp. 1–11.

[18] Bassi, F., Botti, L., Colombo, A., Di Pietro, D. A., and Tesini, P., "On the flexibility of agglomeration based physical space discontinuous Galerkin discretizations," *Journal of Computational Physics*, Vol. 231, No. 1, 2012, pp. 45–65.

[19] Rusanov, V. V., "The calculation of the interaction of non-stationary shock waves and obstacles," *USSR Computational Mathematics and Mathematical Physics*, Vol. 1, No. 2, 1962, pp. 304–320.

[20] Liou, M.-S., "A sequel to ausm: Ausm+," *Journal of computational Physics*, Vol. 129, No. 2, 1996, pp. 364–382.

[21] Pandolfi, M., "A contribution to the numerical prediction of unsteady flows," *AIAA journal*, Vol. 22, No. 5, 1984, pp. 602–610.

[22] Kuzmin, D., "A vertex-based hierarchical slope limiter for p-adaptive discontinuous Galerkin methods," *Journal of computational and applied mathematics*, Vol. 233, No. 12, 2010, pp. 3077–3085.

[23] Persson, P.-O., and Peraire, J., "Sub-cell shock capturing for discontinuous Galerkin methods," *44th AIAA Aerospace Sciences Meeting and Exhibit*, 2006, p. 112.

[24] Hartmann, R., "Higher-order and adaptive discontinuous Galerkin methods with shock-capturing applied to transonic turbulent delta wing flow," *International Journal for Numerical Methods in Fluids*, Vol. 72, No. 8, 2013, pp. 883–894.

[25] Nguyen, C., and Peraire, J., "An adaptive shock-capturing HDG method for compressible flows," *20th AIAA Computational Fluid Dynamics Conference*, 2011, p. 3060.

[26] Lange, M., Knepley, M. G., and Gorman, G. J., "Flexible, scalable mesh and data management using PETSc DMPlex," *Proceedings of the 3rd International Conference on Exascale Applications and Software*, University of Edinburgh, 2015, pp. 71–76.

[27] Balay, S., Abhyankar, S., Adams, M., Brown, J., Brune, P., Buschelman, K., Dalcin, L., Dener, A., Eijkhout, V., Gropp, W., et al., "PETSc users manual," 2019.

[28] Gottlieb, S., and Shu, C.-W., "Total variation diminishing Runge-Kutta schemes," *Mathematics of computation of the American Mathematical Society*, Vol. 67, No. 221, 1998, pp. 73–85.

[29] Spiteri, R. J., and Ruuth, S. J., "A new class of optimal high-order strong-stability-preserving time discretization methods," *SIAM Journal on Numerical Analysis*, Vol. 40, No. 2, 2002, pp. 469–491.

[30] Hascoet, L., and Pascual, V., "The Tapenade automatic differentiation tool: Principles, model, and specification," *ACM Transactions on Mathematical Software (TOMS)*, Vol. 39, No. 3, 2013, p. 20.

Downloaded by Antonietta Conte on September 10, 2019 | http://arc.aiaa.org | DOI: 10.2514/6.2019-4115

[31] Ruf, J. H., McDaniels, D. M., and Brown, A. M., "Details of Side LoadTest Data and Analysis for a Truncated Ideal Contour Nozzle anda Parabolic Contour Nozzle," Tech. rep., 46th AIAA/ASME/SAE/ASEE Joint Propulsion Conference, 2010.

[32] Stark, R., and Hagemann, G., "Current status of numerical flow prediction for separated nozzle flows," Tech. rep., 2ND EUROPEAN CONFERENCE FOR AEROSPACE SCIENCES (EUCASS), 2007.

[33] Schneider, D., and Génin, C., "Numerical Investigation of Flow Transition Behavior in Cold Flow Dual Bell Rocket Nozzles," *51st AIAA/SAE/ASEE Joint Propulsion Conference*, 2015, p. 4219.

[34] Geuzaine, C., and Remacle, J.-F., "Gmsh: A 3-D finite element mesh generator with built-in pre-and post-processing facilities," *International journal for numerical methods in engineering*, Vol. 79, No. 11, 2009, pp. 1309–1331.

[35] Bassi, F., Botti, L., Colombo, A., Crivellini, A., Franchina, N., Ghidoni, A., and Rebay, S., "Very high-order accurate discontinuous Galerkin computation of transonic turbulent flows on aeronautical configurations," *ADIGMA-A European Initiative on the Development of Adaptive Higher-Order Variational Methods for Aerospace Applications*, Springer, 2010, pp. 25–38.

Downloaded by Antonietta Conte on September 10, 2019 | http://arc.aiaa.org | DOI: 10.2514/6.2019-4115